Journal of Carbon Research

MDPI

Article

Acetaminophen Adsorption on Carbon Materials from Citrus Waste

Marwa Gatrouni [1,2], Nedra Asses [3], Jorge Bedia [4,*], Carolina Belver [4], Carmen B. Molina [4,*] and Nadia Mzoughi [1]

[1] Laboratory Research of Science and Technology of Environmental (LRSTE), Higher Institute Science and Technology Environmental À Borj Cédria, University of Carthage, BP-1003, Hammam-Lif 2050, Tunisia; marwa.gatrouni@gmail.com (M.G.); nadia.mzoughi@isste.rnu.tn (N.M.)
[2] Faculty of Science of Bizerte, Department of Chemistry, University of Carthage, Bizerte 7021, Tunisia
[3] Laboratory of Ecologies and Microbial Technology (LETMI), National Institute of Applied Science and Technology (INSAT), University of Carthage, 2 Boulevard de la Terre, B.P. 676, Tunis 1080, Tunisia; nedra.asses@gmail.com
[4] Chemical Engineering Department, Faculty of Sciences, Universidad Autónoma de Madrid, Cantoblanco, 28049 Madrid, Spain; carolina.belver@uam.es
* Correspondence: jorge.bedia@uam.es (J.B.); carmenbelen.molina@uam.es (C.B.M.)

Abstract: Biochar and carbon adsorbents from citrus waste have been prepared by thermal and chemical treatments; they have been used in the aqueous phase adsorption of acetaminophen (ACE) as a model emerging pollutant. These materials were fully characterized by elemental analysis, X-ray fluorescence (TXRF), adsorption/desorption of nitrogen, X-ray diffraction (XRD), Fourier transform infrared spectroscopy (FTIR), point of zero charge (pH_{pzc}), scanning electron microscopy (SEM), and thermogravimetric analyses (TGA/DTG/DTA). A magnetic carbon adsorbent was obtained by $FeCl_3$ activation under an inert atmosphere, giving rise to the best results in ACE adsorption. Adsorption equilibrium data were obtained at 298, 318, and 338 K and fitted to different models, corresponding to the best fitting to the Redlich–Peterson model. The maximum adsorption capacity at equilibrium resulted in 45 mg ACE·g^{-1} carbon at 338 K. The free energy values were calculated, and values between −21.03 and −23.00 kJ·mol^{-1} were obtained; the negative values confirmed the spontaneity of the process. The enthalpy and entropy of the adsorption process were obtained, giving rise to −6.4 kJ·mol^{-1} and 49 J·mol^{-1}·K^{-1}, respectively, indicating a slightly exothermic process and an increase in the randomness at the solid–liquid interface upon adsorption, respectively. The adsorption kinetics were also studied, with the Elovich model being the one that gave rise to the best-fitting results.

Keywords: citrus waste; biochar; carbon adsorbent; acetaminophen; adsorption

Citation: Gatrouni, M.; Asses, N.; Bedia, J.; Belver, C.; Molina, C.B.; Mzoughi, N. Acetaminophen Adsorption on Carbon Materials from Citrus Waste. *C* **2024**, *10*, 53. https://doi.org/10.3390/c10020053

Academic Editors: Miguel A. Montes Morán and Shuguang Deng

Received: 15 March 2024
Revised: 24 May 2024
Accepted: 4 June 2024
Published: 8 June 2024

1. Introduction

Nowadays, agricultural and food processing activities generate huge amounts of solid wastes, which are commonly eliminated by burning, bringing on different ecological and environmental problems [1]. Agricultural waste is cheap, and it includes husks, peels, and shells of different crops such as rice, sunflower, palm, citric, or different kinds of nuts [2–6]. Most of this waste contains such compounds as starch and lignocellulosic biomass including cellulose, hemicellulose, and lignin [7,8], all of them with a high content of carbon, and were easily transformed into activated carbons or biochar under pyrolysis processes [9,10]. Among these agricultural wastes, fruit waste is daily generated all over the world and very often simply dumped into the environment, thus becoming a new source of pollution [11]. Valorization of these agricultural residues is a very interesting approach involving economic, energy, and environmental concerns [12].

Activated carbons are amorphous carbon materials, and some of their main characteristics are a well-developed porous texture and high surface area values [13]. They can

be prepared from biomass by different physical and chemical activation processes [14]. Chemical activation consists of thermal treatment in an inert atmosphere after impregnation of the raw material with an activating agent like $ZnCl_2$, H_3PO_4, or NaOH. $FeCl_3$-activation is a very interesting method of thermal treatment because of the characteristics of the resulting carbons, which have a mainly acidic surface, a pH at the point of zero charge (pH_{PZC}) below 5.0, and the presence of iron species on their surface that gives rise to catalytic and magnetic properties, making their separation from the liquid media after use easier [15–17]. $FeCl_3$ also presents other advantages concerning other chemical activation agents, including lower cost and being more environmentally friendly. Some of the other traditional activating agents (KOH, NaOH, or H_3PO_4) are very strong bases and acids, and their handling requires stricter security measures and materials more resistant to corrosion, thus increasing the cost of the synthesis process [14]. Other possible activating agents, like $ZnCl_2$, show another added problem—as Zn ions and derived oxides are toxic and have to be submitted to stricter discharge regulations [18,19].

This process has been described in three sequential steps: impregnation, thermal activation or pyrolysis, and washing [20,21]. Activated carbons are widely used in different processes such as adsorption [22], as supports of different kinds of catalysts [23,24], and even as bulk catalysts [25,26]. The literature contains numerous works dealing with their use as low-cost adsorbents of very different compounds: dyes [27–29], organic compounds [30,31], heavy metals [32,33], or emerging pollutants (EPs) [34,35]. EPs are defined as chemical compounds that were not previously considered pollutants and, consequently, not included in the current water quality regulations, even though they may pose a potential threat to environmental ecosystems and human health [36]. Among them, hormones, personal care products, household chemicals, endocrine disruptors, and pharmaceuticals can be found in all kinds of water and wastewater [37]. Their removal by adsorption using activated carbons is also well-reported in the literature. Some examples of this process are the adsorption of cephalexin antibiotic on activated carbon from *Arundo donax*—employing different iron salts as activating agents [38]—of ciprofloxacin onto banana peel biochar [10], of antipyrine on activated carbons from $FeCl_3$ activation of Tara gum [39], of sulfamethoxazole antibiotic on an activated carbon obtained through chemical activation of grape seed hydrochars [40], or of acetaminophen by activated carbons obtained from microwave-assisted $FeCl_3$-activation of lignin [15] or Brazil nutshells [41]. Among pharmaceuticals, acetaminophen (ACE) is widely used as an antipyretic, analgesic, and anti-inflammatory, being one of the most common pharmaceuticals found in different aqueous environments [42,43]. It has been reported in the literature that ACE is a wastewater pollutant in around 29 countries [44]. Very high concentrations of this pharmaceutical have been detected in wastewater in Canada (461 μL^{-1}) or India (up to 868 μL^{-1}) [45,46], constituting a representative example of a pollutant to be eliminated by adsorption from wastewater.

The aim of this study is the valorization of citrus waste into biochars and carbon adsorbents by physical (thermal treatments at different temperatures) and chemical processes ($FeCl_3$-activation) and their use as adsorbents in the removal of acetaminophen drug as a model emerging pollutant, from aqueous solutions by adsorption. Citrus waste has been scarcely tested in the literature to give rise to carbon adsorbents that are able to remove emerging pollutants by adsorption. Moreover, in this case, magnetic carbon was obtained, assuming a great advantage in its practical use. The effect on the adsorption capacity of initial pH, ACE concentration, and adsorption temperature was investigated. The most promising carbon adsorbent was further used for adsorption equilibrium and kinetic studies.

2. Materials and Methods

2.1. Raw Materials

The chemicals and reagents used, namely iron chloride ($FeCl_3$), sodium hydroxide (NaOH), hydrochloric acid (HCl), and sodium chloride (NaCl), were of analytical grade

and purchased from Sigma-Aldrich (Madrid, Spain). The origin of the citrus waste was mainly a mix of different kinds of Tunisian oranges.

2.2. Synthesis of Biochar and Carbon Adsorbents

Figure 1 schematizes the different routes used for the synthesis of the biochar and carbon adsorbents. First, the waste biomass citrus was dried at 378 K to remove the moisture. The resulting solid was crushed into a powder, sieved at 0.150 mm, and used for the synthesis of the different biochar and carbon adsorbents. Citrus-derived biochar (BC) was prepared by carbonization at 973 K for 2 h. The carbonization temperature was reached at a heating rate of 10 K·min^{-1}, and all the process was performed in an N_2 atmosphere (150 mL STP·min^{-1}). A carbon sample (AC) was synthesized by chemical activation with $FeCl_3$. Briefly, 30 g of dried biomass was added to 150 mL of an aqueous solution containing 30 g of $FeCl_3$.6 H_2O, and the mixture was maintained under stirring for 2 h. Next, the solid was filtered and washed with water at 353 K until the pH of the solution was 7 (the initial pH of the solution was 2). Finally, the solid was separated by filtration and carbonized in an N_2 atmosphere (150 mL STP·min^{-1}) at 773 K for 2 h. Lastly, a magnetic carbon (MAC) was prepared by thermal treatment to AC at 1173 K (heating rate 283 K·min^{-1}) for 2 h under N_2 atmosphere (150 mL STP·min^{-1}). This MAC sample showed magnetic properties similar to those of other activated carbons synthesized by $FeCl_3$ activation [47].

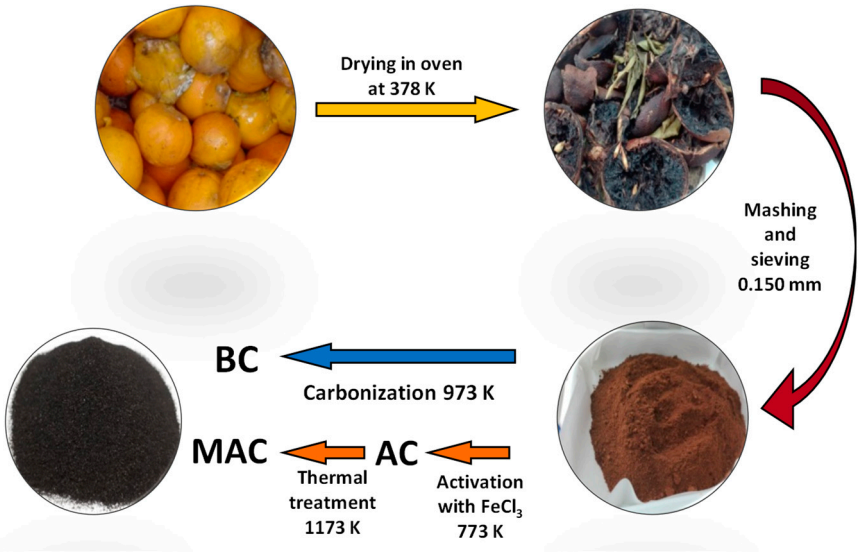

Figure 1. Preparation of the biochar and carbon adsorbents used in this work.

2.3. Characterization

Elemental analyses were carried out to determine the C, N, S, and H contents with a Perkin Elmer elemental analyzer (210 CHN model). The metal content of the catalysts was measured by X-ray fluorescence with a TXRF EXTRA-II spectrometer (Rich and Seifert, Ahrensburg, Germany). The samples were previously submitted to an acid treatment (aqua regia mixture) at 373 K. A Micromeritics Tristar 3020 apparatus was used to obtain the N_2 adsorption/desorption isotherms at 77 K after degasification of the carbons at 433 K and 5×10^{-3} Torr for 16 h. Specific surface areas were obtained using the BET method. The pore size distribution was calculated using density functional theory (DFT) [48].

The XRD patterns of the carbon adsorbents prepared were obtained with a Siemens model D-5000 diffractometer using CuKα as radiation source (scan speed of 0.05°/s, 2θ range from 3 to 80°). The surface functional group identification in the spectral range from 4000 to 450 cm^{-1} was obtained using an FTIR spectrophotometer (Perkin Elmer Spectrum IR Version 10.6.0). The point of zero charge (pH_{pzc}) of the adsorbents was determined using the pH-drift method [49]. The morphological features were analyzed using scanning electron microscopy (SEM) with a Philips XL20 scanning electron microscope at an accel-

erating voltage of 20 kV. Samples were previously coated using an Edwards (UK) Auto 306 vacuum coater with silver as the coating agent. Finally, thermal gravimetric analysis (TGA/DTG) and differential thermal analysis (DTA) were performed in the temperature range of 298–1223 K using Perkin Elmer (Waltham, MA, USA) TGA7 and DTA7 devices with a heat rate of 10 K/min. The samples, with masses ranging between 5 and 10 mg, were placed in the TGA using alumina pans with a capacity of 70 mL. The accuracy of temperature was 0.1 K, while for mass measurements, it was 10^{-3} mg. The magnetic characteristics of MAC were determined using a magnetometer (MPMS-XL of Quantum Design, with SQUID detector) at room temperature. The hysteresis loop used to study the magnetic properties of the carbon adsorbent was collected on a variable field translation balance (MAG Instruments, Gyor, Hungary) at 300 K with a maximum field of 5000 Oe.

2.4. Adsorption Tests

Adsorption of acetaminophen was carried out in the aqueous phase using the prepared materials. In the first stage, batch equilibrium experiments were developed at different temperatures (298, 318, and 338 K) using 50 mL of aqueous solutions with different initial concentrations of acetaminophen in the range of 10 to 75 mg·L^{-1} with a carbon dose of 0.2 g·L^{-1}. Next, while stirring at a controlled temperature in an orbital shaker at 200 rpm for 24 h was performed, the liquid phase was filtered (Whatman®, membrane filters PTFE, 0.45 µm pore size) and, subsequently, analyzed. Kinetic adsorption tests were also carried out with an initial acetaminophen concentration of 25 mg·L^{-1}, the same solution volume, carbon adsorbent concentration, and the temperatures mentioned above for the equilibrium tests in a similar batch system. The regenerability and reusability of the MAC material were assessed by conducting six cycles of the adsorption/desorption process. After each cycle, the adsorbent was recovered using centrifugation, washed with hot water (333 K) for 1 h, and, finally, dried at 353 K. All the adsorption tests were performed in triplicate, and deviations lower than 10% were obtained. The represented values correspond to the mean values.

The acetaminophen concentration was quantified by HPLC (Shimadzu Prominence-I LC-2030C apparatus) with a diode array detector (SPD-M30A) and a reverse phase C18 column (Eclipse Plus 5 µm, Agilent Technologies, Madrid, Spain) at the maximum acetaminophen absorption (wavelength of 246 nm). A mixture of acetonitrile/acetic acid 0.1% *v/v* solutions was employed as a mobile phase using a gradient method (10/90 to 40/60% for 17 min) with a constant flow of 0.7 mL·min^{-1}. The adsorption capacity at any time (t) and at equilibrium were calculated using Equations (1) and (2), respectively:

$$q_t = \frac{V}{m}(C_0 - C_t) \quad (1)$$

$$q_e = \frac{V}{m}(C_0 - C_e) \quad (2)$$

where $\mathbf{q_t}$ (mg/g) is the adsorption capacity at any time, $\mathbf{q_e}$ (mg/g) is the adsorption capacity at equilibrium, **V** is the solution volume (L), and **m** is the adsorbent dose (g).

3. Results and Discussion

3.1. Precursor Characterization

Figure 2a represents the thermogravimetry (TGA) and difference thermogravimetry (DTG) profiles of citrus waste obtained under an air atmosphere. Different mass losses were observed in this TGA at different temperature ranges. The first mass loss, below 408 K (3.2% mass loss), is attributed to the evaporation of water. Other mass losses at different temperatures (408–515 K (18.8%), 515–556 K (19.6%), 556–649 K (25.1%) and 649–704 K (9.5%)) correspond to the thermal decomposition of the hemicellulose, cellulose and other organic compounds, being the decomposition of hemicellulose and cellulose molecules mainly leading to the release of volatile matter. The last mass loss between 704 and 791 K (21.1%) is due to the slower oxidation of lignin due to its complex structure. At the end

of the oxidation, the material remained as ashes (c.a. 2 wt%). DTA thermograms of citrus waste can also be used to determine qualitatively the heat absorbed or released by the sample during the various stages of decomposition. Figure 2b shows the DTA curve of the raw material under an oxidative atmosphere of air. In this figure, different peaks can be observed: an endothermic peak at 339 K attributed to the evaporation of the water, exothermic peaks at 473, 523, 583, and 683 K corresponding to the decomposition of organic compounds leading to the formation and combustion of volatile products. Finally, an exothermic peak at 773 K is attributed to the oxidation of lignin.

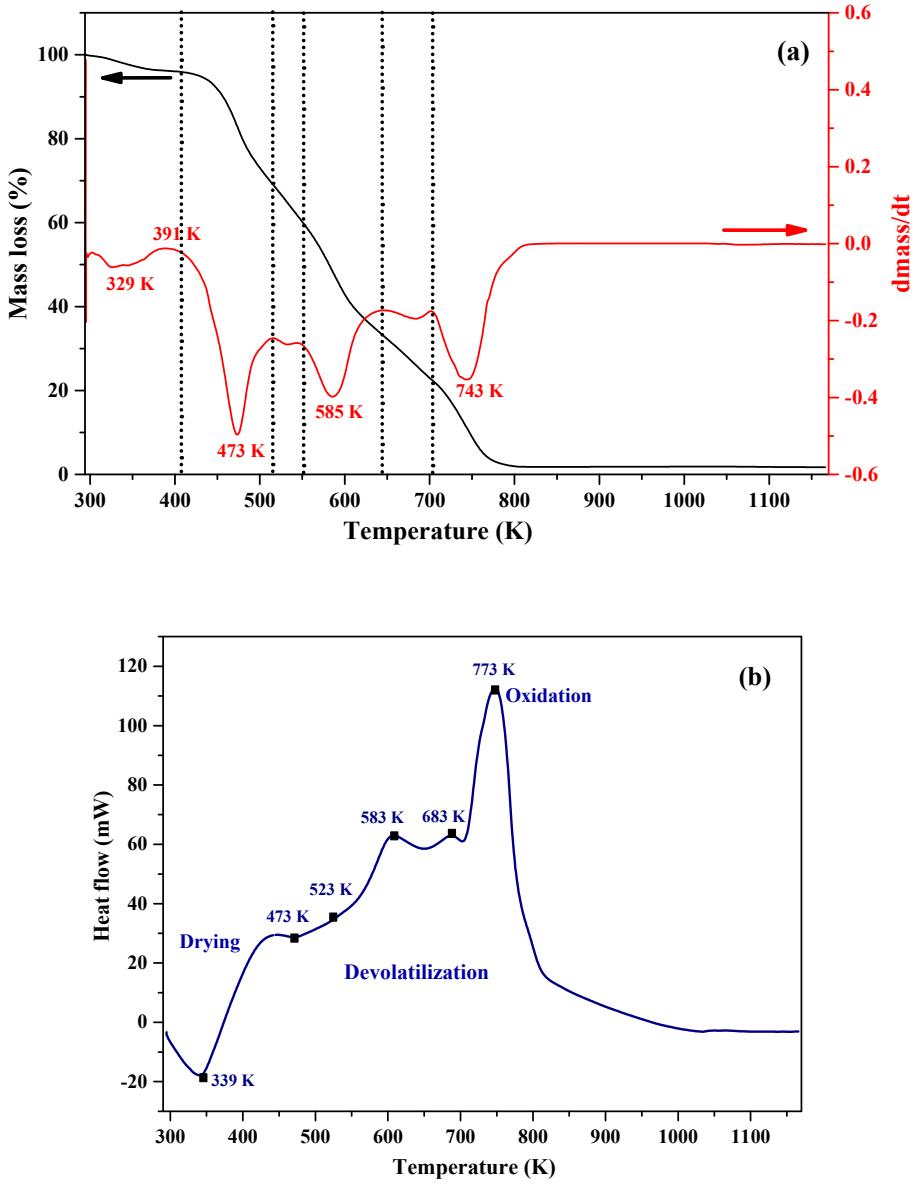

Figure 2. (**a**) TGA (black) and DTG (red) profiles and (**b**) DTA of citrus waste under an air atmosphere at a heating rate of 10 K·min^{-1}.

3.2. Adsorbents Characterization

Table 1 summarizes the mass yield, calculated as the ratio between the final mass of the sample referred to the mass of citrus waste used in the different synthesis processes. The synthesis of the biochar (BC) resulted in a 31.2% yield as a consequence of the release of volatile organic matter during the heat treatment at 973 K. In the case of the carbon (AC), a significantly higher yield was obtained as a consequence of both of the following: (i) The lower temperature used in the activation process than in the synthesis of the biochar (773

versus 973 K, respectively); (ii) Mainly reactions of depolymerization, dehydration, and condensation that take place for restricting the formation of tars and volatile matter during the chemical activation process with $FeCl_3$ [14]. The yield of the synthesis of the magnetic carbon (MAC) is slightly lower than that of the AC due to the deeper devolatilization between 773 and 1173 K. The ash and elemental (C, H, N, O, and Fe) content of the samples is included in Table 1. As can be seen, all the adsorbents show a high percentage of carbon (between 65 and 79%) in their structure, as expected for carbon-based adsorbents. It is noteworthy that the increase in the ash content after activation with $FeCl_3$ can be observed for both AC and MAC samples. This is most likely due to the following: (i) The devolatilization of the organic precursor during the thermal treatments; (ii) The incorporation of part of the iron used in the activation process to the structure of these adsorbents, as supports the increase in the iron content quantified by TXRF.

Table 1. Mass yield, elemental (C, H, N; O, d.a.f.), TXRF (Fe) analyses, and ash content.

Sample	Yield (%)	C (wt%)	H (wt%)	N (wt%)	O * (wt%)	Ash (wt%)	Fe (wt%)
BC	31.2	78.8	1.8	1.9	11.0	6.5	0.02
AC	45.6	65.3	2.0	1.7	15.8	15.2	13.5
MAC	41.4	72.9	1.5	1.1	4.9	19.6	16.7

* by difference.

Figure 3a displays the N_2 adsorption/desorption isotherms of the three synthesized samples. In the case of biochar (BC), a very low amount of N_2 is adsorbed due to the low porosity development obtained in the carbonization process in the absence of an activating agent. The isotherms of both carbons, AC and MAC, correspond to type I according to IUPAC classification characteristics of microporous materials. Usually, the activation with $FeCl_3$ using a wet impregnation method results in the generation of microporosity, most likely due to the relatively low presence of the activating agent during the carbonization process [14]. Table 2 summarizes the values of the BET and micropore surface areas and the total pore volumes. The active samples show a significant porous development with BET surface areas of around 280 $m^2 \cdot g^{-1}$. The surface area values found in this work are lower than most of the activated carbons. However, these values are in the order of other carbon adsorbents obtained from different natural residues reported in the literature: da Silva et al. [5] found surface area values in the range 166–400 m^2/g for carbons obtained from citrus fruit residues, Verma et al. [11] found values of 207 m^2/g and 37 m^2/g for carbon adsorbents derived from waste biomass of citrus limetta (peel and pulp), Kumar et al. [6] found 67.5 m^2/g for biochars obtained from orange peel residues, Ahmadian et al. [2] found 195 m^2/g for biochars obtained from lemon peel and Aboli et al. [50] found 7.2 m^2/g for carbons prepared from citrus limetta leaves. It should be remarked that the impregnation step, the mixture of the carbonaceous precursor with $FeCl_3$, is usually performed by two different methods: in an aqueous solution or by physical mixing between the carbon precursor and the iron chloride activating agent. In the aqueous solution selected in this study, the carbonaceous precursor is suspended under stirring in an aqueous solution of $FeCl_3$. On the other hand, the physical mixing impregnation procedure consists of mixing the solid state of both the carbonaceous precursor and the iron chloride in a specific impregnation ratio. In this case, it is advisable to perform a grinding of both materials to ensure better contact between them. In this study, we selected the aqueous solution mixture, which usually leads to less development of porosity, although it is simpler to perform in real applications.

On the other hand, in all cases, most of the pores show sizes below 2 nm, with a mean pore size of around 1 nm, indicative of the high microporosity of these materials (Figure 3b). However, while the pore-size distribution of the MAC material is characterized by a unimodal distribution centered at around 1 nm, a bimodal distribution was obtained for AC with a maximum peak also around 1 nm and a lower second peak around 1.5 nm.

BC material also shows a bimodal pore-size distribution with less intense peaks of around 1 and 1.2 nm and a wide band from 4 to 10 nm, pointing to some kind of mesoporosity, as was confirmed by its low micropore surface area (Table 2).

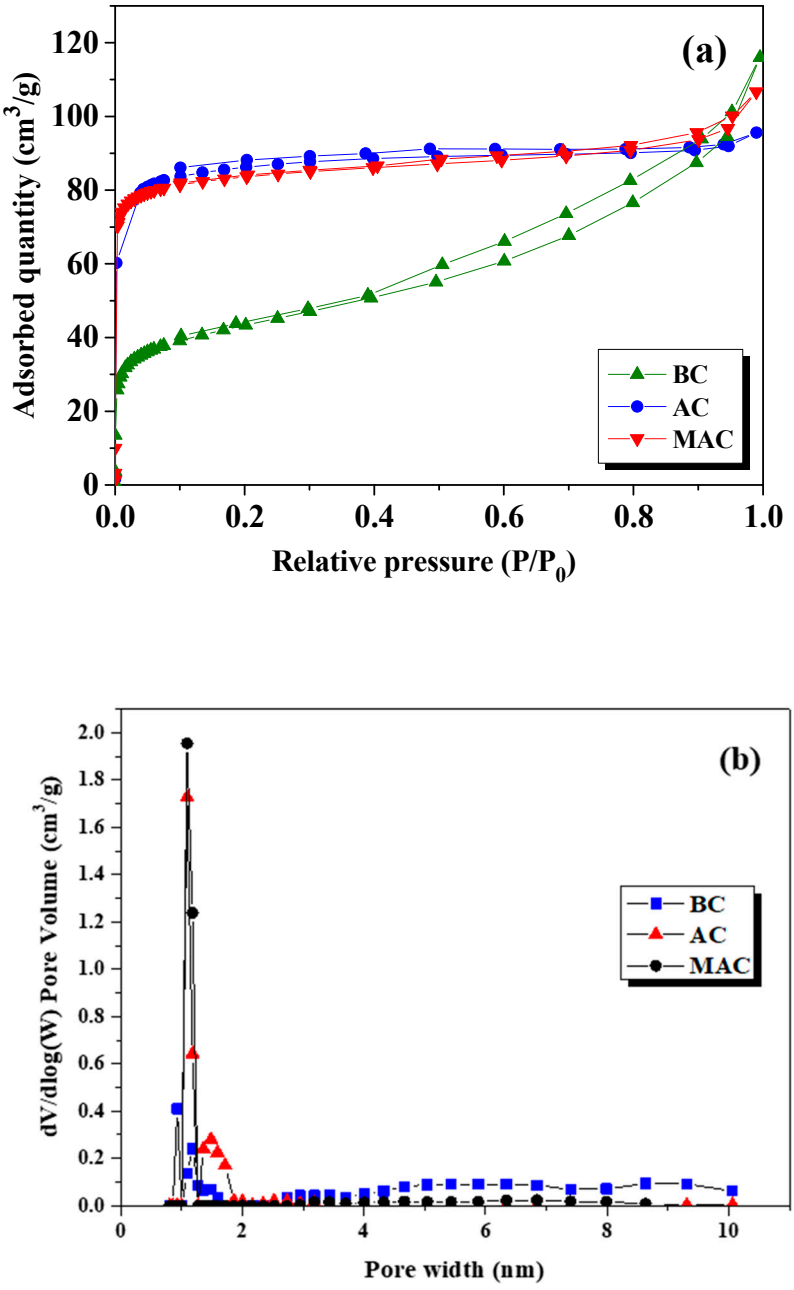

Figure 3. (**a**) N_2 adsorption/desorption isotherms at 77 K. (**b**) Pore size distribution of the materials prepared in this work.

Table 2. Textural parameters.

Sample	S_{BET} ($m^2 \cdot g^{-1}$)	Micropore Surface [a] ($m^2 \cdot g^{-1}$)	V_{total} [b] ($cm^3 \cdot g^{-1}$)
BC	148	57	0.08
AC	280	234	0.10
MAC	273	232	0.11

[a] Micropore surface area from t-method; [b] Total pore volume at P/P_0 equal to 0.99.

Figure 4 represents the XRD patterns of the different samples. In the case of the BC sample, a broadband can be observed at around 24° corresponding to (002) stacking of the graphitic basal plan in biochar. In addition, a well-defined peak is obtained at 29.5°, which is associated with the presence of calcite ($CaCO_3$), and commonly present in biomass-derived chars [51]. This XRD pattern is characteristic of a predominantly amorphous structure, with the presence of some well-defined peaks associated with the inorganic matter present in the raw biomass, in this case, citrus waste. After activation, no broad peak associated with the presence of graphite disappears completely as a consequence of the disorder of the graphene layer, which results in the development of porosity [52]. Sharp and narrow peaks were obtained in the MAC sample and less intense in the AC sample that can be assigned to Fe_3O_4 (JCPDS #75-0033) at 30.2°, 35.7° and 57.2° and to γ-Fe_2O_3 (JCPDS #39-1346) at 43.4°, 53.8° and 63.0° [53,54]. Moreover, undefined iron oxides can also be found according to the database JCPDS#82-1533 at 2θ values around 33.5°, 35.9°, 49.7°, 54.3°, and 62.6° [55,56]. The increase in the intensity of iron peaks in the MAC sample indicated a higher crystallinity of the iron species in this sample, most likely due to the high temperature achieved during the preparation of this carbon (1173 K).

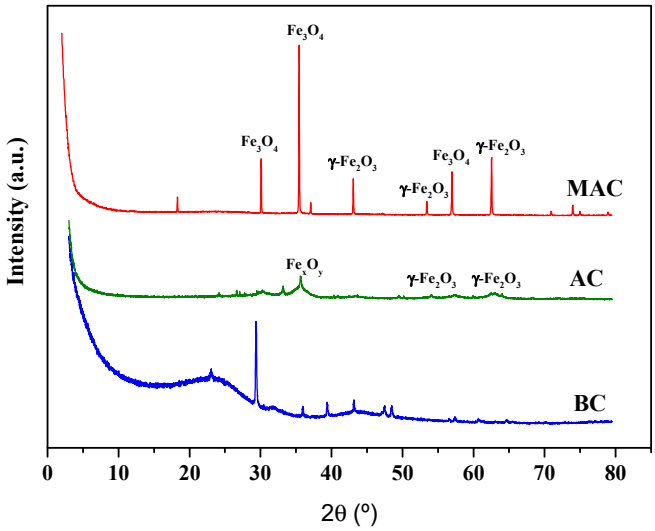

Figure 4. X-ray diffractograms.

Figure 5 shows the FTIR spectra of AC and MAC samples. The most evident difference between both spectra is the decrease in the intensity of the bands between 900 and 1600 cm^{-1} of the MAC spectrum. This is due to the loss of most of the oxygen surface groups of the MAC sample during the treatment at 1173 K (confirmed by the reduction in the oxygen content, Table 1). The main bands observed in both samples are around 2320 cm^{-1} due to the asymmetric stretching vibrations of CO_2 [57,58], 1570 cm^{-1} due to OH bending [54], and around 1170 cm^{-1} due to the stretching vibrations of C–OH bonds [59]. Other less intense bands are observed at lower wavelengths. The bands between 500 and 800 cm^{-1} are related to the C–O and metal-oxygen (Fe–O) bonds of the Fe_3O_4 group [55]. Bands around 550 cm^{-1} are associated with the M-O band (Fe–O in this case), while those around 600 cm^{-1} can be assigned to Fe_3O_4 particles on the surface [60].

The adsorption of different solutes on the surface of the adsorbents is highly dependent on the pH of the solution as well as the pH of point zero charges (pH_{pzc}) of the adsorbent used. The adsorbent surface is negatively charged when the solution pH is higher than the pH_{pzc} of the adsorbent and positively charged when it is lower [61]. The pH_{pzc} of the adsorbents prepared was measured, and the results are shown in Figure 6. The pH_{pzc} values were 8.9, 6.4, and 4.3 for BC, AC and MAC, respectively. The values agree well with those previously obtained for activated carbons synthesized by chemical activation with $FeCl_3$ [15]. Regarding the adsorbate behavior, acetaminophen molecules behave as weak

acids with a pK_a of 9.38, so at pH values below the pK_a, this compound is predominantly in its neutral form. The adsorption tests in this work were carried out at natural pH values of acetaminophen aqueous solutions (6.3–7.2). In these conditions, the BC will be negatively charged, AC will be weakly charged since the pH of the solution and the pH_{pzc} are very similar, and, finally, MAC will be positively charged [62]. On the other hand, acetaminophen will be in molecular form (uncharged), and, therefore, adsorption should not be controlled by electrostatic attraction, as has been previously reported in the literature [63].

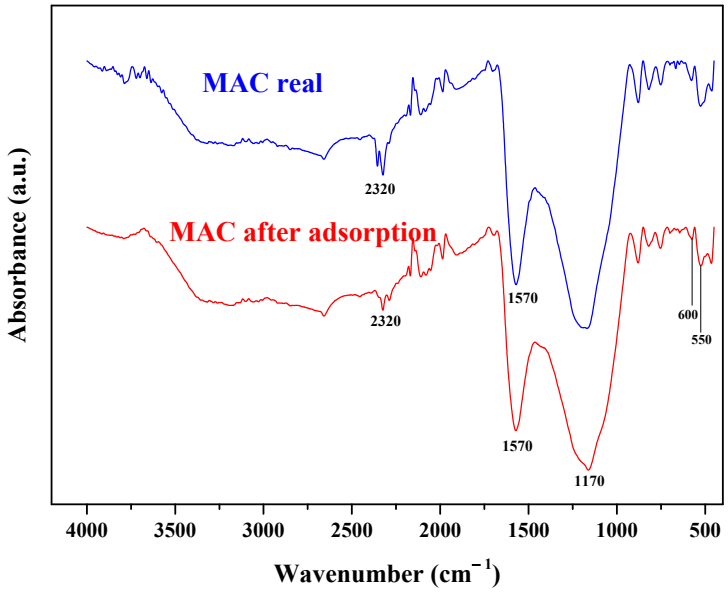

Figure 5. FTIR spectra of AC and MAC.

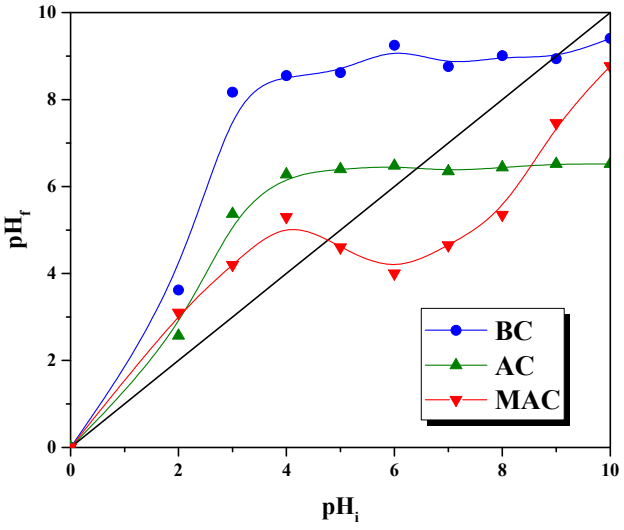

Figure 6. pH_{pzc} values.

Figure 7 shows SEM images of BC and AC carbons (MAC was not analyzed due to its magnetic nature). The BC sample shows a homogeneous surface with a scarcity of defects, in contrast to AC, which shows a very inhomogeneous surface with many small and irregular particles, more characteristic of a disordered material. These morphologies seem to agree with the porous characteristics of both materials, being BC predominantly non-porous and thus with a homogeneous surface, and AC a material with a more developed porosity and, consequently, a more irregular and disorganized morphology.

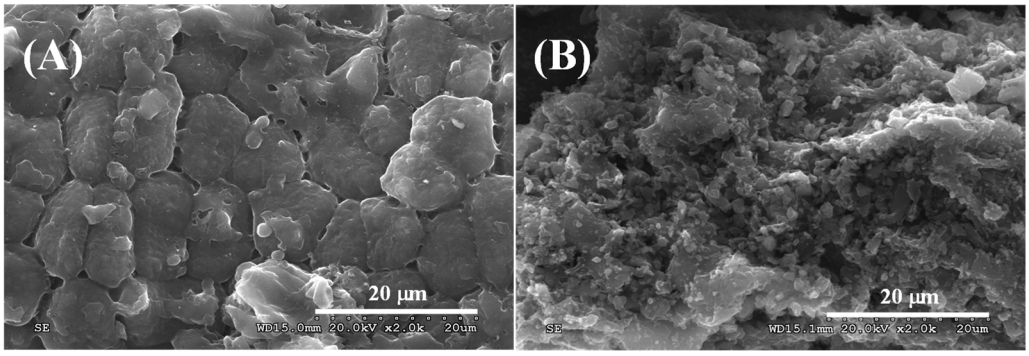

Figure 7. SEM images of (**A**) BC and (**B**) AC.

The magnetic properties of the MAC (Figure 8) were studied using the magnetic hysteresis curves obtained, the most important characteristics of a magnetic material, yielding magnetic indicators including the coercive force (Hc), saturation magnetization (Ms) and remanent magnetization (Mr), [27]. As in previous works [27,64], an obvious hysteresis loop is difficult to detect at the full scale, indicating the superparamagnetism of the MAC material. The maximum saturation magnetization of MAC was 28.57 emu·g^{-1}, which indicates that the solid could be separated from the liquid phase by using a magnet. It should be remarked that this value is higher than those of many other magnetic-activated carbons reported in the literature. In this sense, [60] reported a saturated magnetization of only 4.47 emu·g^{-1} at 300 K for activated carbons from almond shells, while a value of 2.352 emu·g^{-1} was found for sludge biomass-derived activated carbon [49,65] or 14.26 emu·g^{-1} for coal-based magnetic activated carbons [66]. More similar magnetization values of 28.7 emu·g^{-1} for a magnetic activated carbon derived from a biomass waste [18,29], 34.7 emu·g^{-1} for γ-Fe_2O_3/carbon hollow spheres [64], or 30.37 emu·g^{-1} for eucalyptus sawdust magnetic activated carbon [27] were reported in the literature. It is worth mentioning that considering the values of coercivity (Hc = 38.25 Oe), remanence (Mr = 1.97 emu g^{-1}), and the ratio between remanence and saturation magnetization (6.9%), it can be confirmed that the sample possesses superparamagnetic properties at room temperature, as the Mr/Ms ratio is lower than 25% [67].

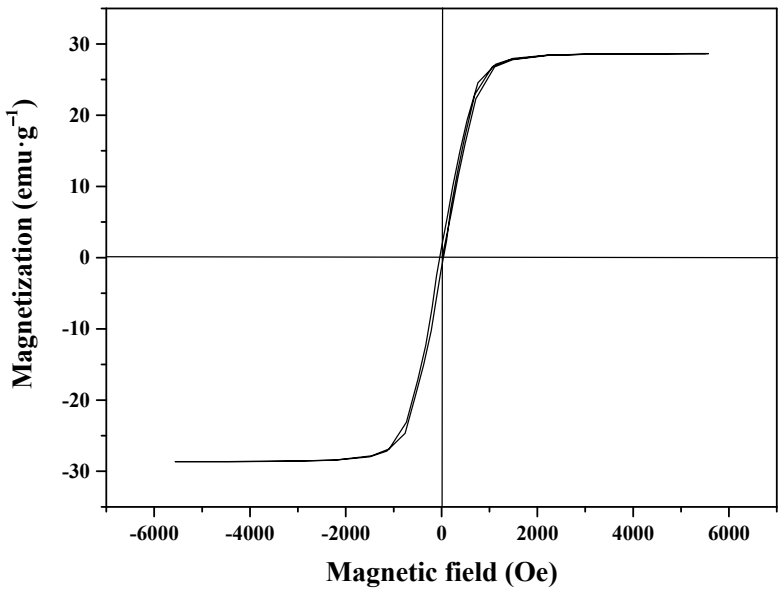

Figure 8. Magnetization curve of MAC.

3.3. Acetaminophen Adsorption

Figure 9 represents the ACE adsorption kinetics at 298 K on BC, AC, and MAC carbon adsorbents. While BC only achieved around 50% of ACE removal, both samples, AC and MAC, reached the complete ACE elimination of the final effluent, probably due to the most developed porous structure of these two materials. It should be underlined that magnetic carbon (MAC) shows faster adsorption kinetics. Anyway, all the samples show a relatively fast adsorption process, reaching the equilibrium after 5 min in the case of the MAC sample, around 10 min for BC, and 30 min for AC. Behavior was also observed for other carbon adsorbents obtained from biomass precursors for ACE adsorption [41]. These results suggest that the carbon adsorbents have a large number of adsorption sites unoccupied, leading to a high driving force for the mass transfer from the bulk solution to the surface of the adsorbent and, consequently, to a fast adsorption process [68,69].

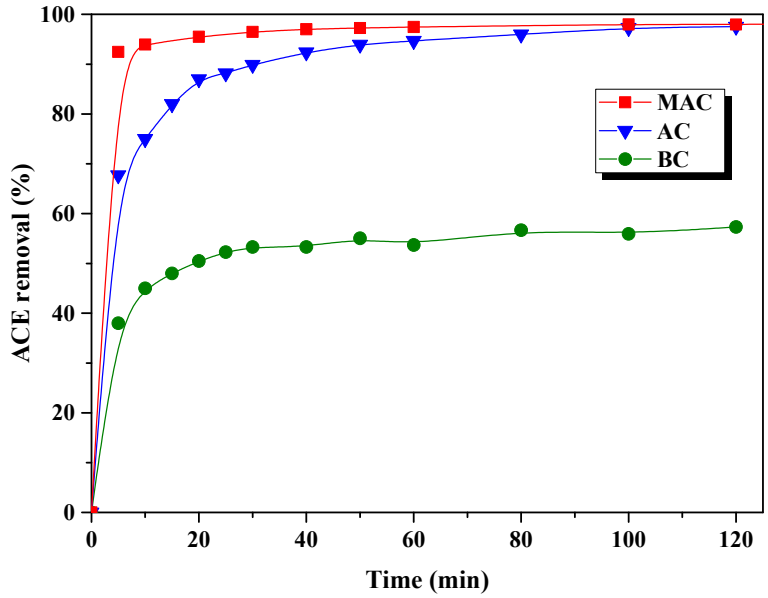

Figure 9. ACE adsorption kinetics (adsorbent mass = 0.2 g·L^{-1}, [ACE]$_0$ = 5 mg·L^{-1}; T = 298 K).

Considering that the MAC yielded the best results in ACE adsorption and presented the intrinsic advantage of its easier separation of the effluents due to its magnetic properties, the rest of the study was performed with this adsorbent. Figure 10 represents the ACE equilibrium adsorption capacities at different initial pH values. As can be seen, the adsorption capacities are stable in a wide pH range. Only at high pH values, with a strong basic solution, is a very significant decrease in the adsorption capacity observed. This is likely due to the changes in the electrostatic adsorbate–adsorbent forces with pH. At pH higher than 9.5 (the pKa values of ACE), both the ACE molecules and the MAC surface are negatively charged. Thus, certain repulsive electrostatic forces are expected, which justifies the observed reduction in the adsorption capacities at the highest pH analyzed.

In the literature, it is reported that, in the case of activated carbons, ACE adsorption occurs through H-bonding, π-π electron donor-acceptor, n-π donor-acceptor, and π-H bonding [70]. Nguyen et al. [63] include a deep study of the ACE adsorption mechanism onto carbonaceous materials: the adsorption process of polar aromatic pollutants like ACE in solution onto porous carbonaceous materials (biochar or activated carbon) often combines many interactions (or mechanisms) such as electrostatic attraction, van der Waals force, ion exchange, hydrogen bonding formation, n-π interaction, π-π interaction and pore-filling [71,72]. In this sense, the pore filling has been reported in the literature as the dominant adsorption mechanism of ACE onto carbonaceous adsorbents [73]. However, the primary adsorption mechanism is often strongly dependent on the conditions of the adsorption study (i.e., solution pH, temperature, and initial adsorbate concentration),

adsorbate characteristics (i.e., molecular size, solubility, pKa, and electron distribution) and adsorbent properties (i.e., surface area, pore size distribution, and surface functional groups). To learn more in-depth about the main reaction mechanism of the adsorption process developed in this study, the BET analysis of the MAC carbon after acetaminophen adsorption was carried out. The BET surface area value decreased from 273 $m^2 \cdot g^{-1}$ to 22 $m^2 \cdot g^{-1}$. This result agrees with previous works where also a dramatic decrease in the adsorbent surface area of a commercial AC was achieved after acetaminophen adsorption, from 1248 to 45.6 m^2/g [63], suggesting that pore filling plays a more significant role in the uptake process than other mechanisms although the influence of another type of electrostatic interaction cannot be completely ruled out.

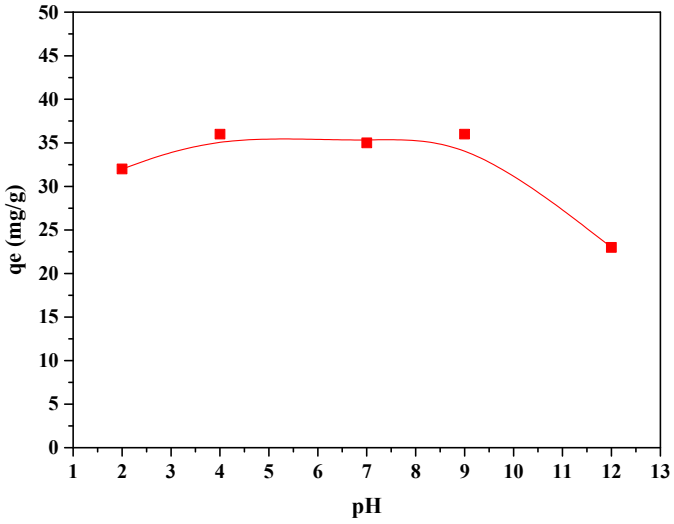

Figure 10. ACE equilibrium adsorption capacities on MAC at different initial pH values (adsorbent mass = 0.2 $g \cdot L^{-1}$, $[ACE]_0$ = 25 $mg \cdot L^{-1}$; T = 298 K).

To evaluate the reusability of the MAC material, it was reused in six successive runs at 338 K, and its adsorption capacity at equilibrium was tested (Figure 11). Adsorption capacity was maintained at around 87% after six successive cycles, confirming the high stability of this carbon and that desorption is feasible and successfully performed.

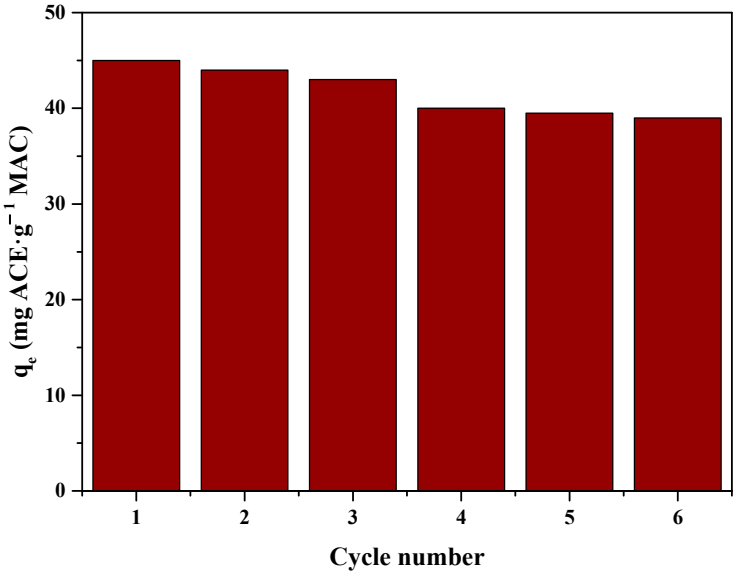

Figure 11. MAC reusability tests (adsorbent mass = 0.2 $g \cdot L^{-1}$, T = 338 K).

3.3.1. Adsorption Kinetics

ACE adsorption kinetics on MAC at different temperatures are collected in Figure 12. The adsorption process is very fast regardless of the adsorption temperature in the range studied. The adsorption capacity increases slightly with the temperature, suggesting an adsorption process of endothermic nature.

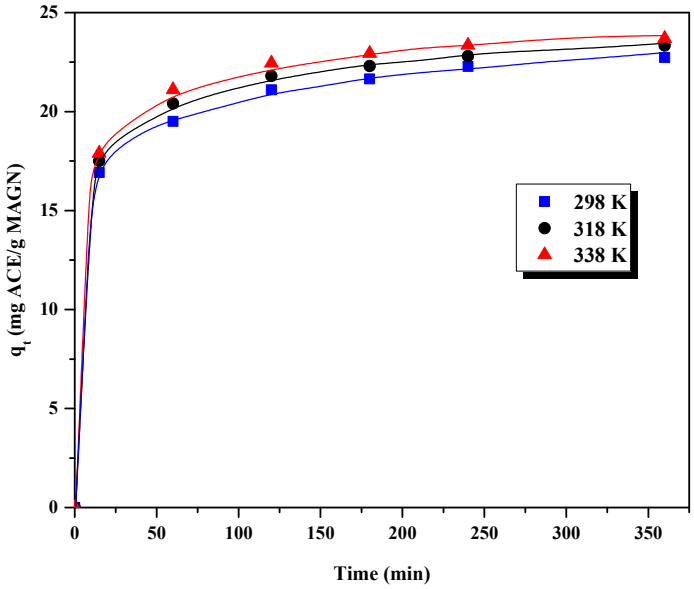

Figure 12. ACE adsorption kinetics on MAC at different temperatures (adsorbent mass = 0.2 g·L^{-1}, [ACE]$_0$ = 25 mg·L^{-1}). Experimental points and fitting curves to Elovich model.

The kinetic data were fitted to four well-known kinetic models [74], namely pseudo-first-order (Equation (3)), pseudo-second-order (Equation (4)), intraparticle diffusion (Equation (5)) and Elovich (Equation (6)) models, whose equations are shown below.

$$q_t = q_e\left(1 - e^{-k_1 t}\right) \quad (3)$$

$$q_t = \frac{k_2.q_e^2.t}{1 + k_2 q_e t} \quad (4)$$

$$q_t = k_p t^{1/2} + C \quad (5)$$

$$q_t = \frac{1}{\beta}\ln(1 + \alpha\beta t) \quad (6)$$

where $\mathbf{q_t}$ (mg·g^{-1}) is the amount of acetaminophen adsorbed at a specific time, $\mathbf{q_e}$ (mg·g^{-1}) is the amount of acetaminophen adsorbed at equilibrium; $\mathbf{t}$ (min) is the adsorption time; $\mathbf{k_1}$ (min^{-1}) is the pseudo-first-order model rate constant, $\mathbf{k_2}$ (g·mg^{-1}·min^{-1}) is the pseudo-second-order model rate constant, $\mathbf{k_p}$ (mg·g^{-1}·min$^{-0.5}$) is the rate constant of the intraparticle diffusion model, C (mg·g^{-1}) is a constant related to the thickness of the boundary layer, $\boldsymbol{\alpha}$ (mg·g^{-1}·min^{-1}) is the Elovich initial rate constant and $\boldsymbol{\beta}$ (g·mg^{-1}) is the desorption constant. Table 3 summarizes the values of the parameters of each model obtained by non-linear fitting of the experimental data shown in Figure 12 as well as their corresponding correlation coefficients. All the models provided good fitting with high correlation coefficients (higher than 0.99) except the pseudo-first-order model. Elovich's model gave rise to the best fitting of the experimental data with the highest values of these correlation coefficients and is represented in Figure 12, followed very near the pseudo-second-order model. In previous studies, these two models have also yielded the best fitting to the experimental adsorption kinetics data. Gómez-Avilés et al. [15], using activated carbons obtained from microwave-assisted $FeCl_3$-activation of lignin, found slightly better results

for the pseudo-second-order model, while this model was selected by Chen et al. [27] with a eucalyptus sawdust magnetic activated carbon and Ibrahim et al. [55] using a biogenic iron permeated activated carbon derived from sweet lime waste. In all these cases, adsorption on different activated carbons fitted to the pseudo-second-order kinetics model to describe the adsorption kinetics data for the entire sorption period, suggesting that the pseudo-second-order adsorption mechanism was predominant. Usually, the pseudo-first-order kinetic equation was more suited to describe the kinetics of the initial stage with some limitations in its application, while the pseudo-second-order kinetic equation contained the complete adsorption processes, such as surface adsorption, membrane diffusion, internal diffusion, etc., being more suitable for the adsorption process [27]. Other authors have also found the best fitting of the experimental data to the Elovich model but always followed very near the pseudo-second-order adsorption model using different adsorbents: magnetic activated carbon–cobalt nanoparticles [75] or activated carbon prepared from Brazil nut shells [76].

Table 3. Kinetic model parameters of ACE adsorption on MAC.

Model	T (K)	q_e (mg·g^{-1})	k_1 (min^{-1})	R^2
Pseudo-first order	298	21.5	0.1022	0.9843
	318	22.1	0.1032	0.9882
	338	22.7	0.1024	0.9910
Model	**T (K)**	**q_e (mg·g^{-1})**	**k_2 (g·mg^{-1}·min^{-1})**	**R^2**
Pseudo-second order	298	22.4	0.0084	0.9948
	318	23.0	0.0085	0.9968
	338	23.6	0.0084	0.9982
Model	**T (K)**	**k_p (mg·g^{-1}·min$^{-0.5}$)**	**C (mg·g^{-1})**	**R^2**
Intraparticle difusion	298	0.383	16.2	0.9953
	318	0.373	17.0	0.9944
	338	0.368	17.6	0.9924
Model	**T (K)**	**α (mg·g^{-1}·min^{-1})**	**β (g·mg^{-1})**	**R^2**
Elovich	298	1040.1	0.5318	0.9997
	318	1718.0	0.5396	0.9996
	338	2232.5	0.5378	0.9988

3.3.2. Adsorption Equilibrium and Thermodynamics

Figure 13 displays the ACE equilibrium adsorption isotherms on MAC at 298, 318, and 338 K. They belong to the L type of Giles classification [77], common in liquid-phase adsorption, and characteristic of strong adsorbate–adsorbent attractive forces and weak interactions between the adsorbate molecules. As can be observed, the amount of ACE adsorbed at equilibrium increased with temperature, in agreement with the kinetic curves (Figure 12) and suggesting an endothermic character of the process. This behavior has been previously reported in the literature for the adsorption of ACE on other biomass-derived activated carbons [78], although other authors have reported just the opposite behavior with other activated carbons [79,80]. These differences could be due to the differences in the adsorbent surface chemistry [78]. The highest adsorption capacity at equilibrium is around 45 mg·g^{-1}. These values agree with others found in the literature for activated carbons prepared from different biomass precursors for ACE adsorption, such as 19.7 mg·g^{-1} for pyrolyzed pulp mill sludge [81], 20.96 mg·g^{-1} for rice husk [82] or 45.45 mg·g^{-1} for oak fruits [83]. In general trend, activated carbons with more developed surface area achieved higher equilibrium adsorption capacities: different activated carbons with surface area values in the range 400−1000 m^2·g^{-1} yielded adsorption capacities of 118.6 mg·g^{-1} for AC from industrial pre-treated cork [84] or 190 mg·g^{-1} for activated carbons from sisal waste [85]. This fact suggests that, despite other characteristics of the adsorbent that can

affect the adsorption process, the porosity development is among those that most affect the adsorption process.

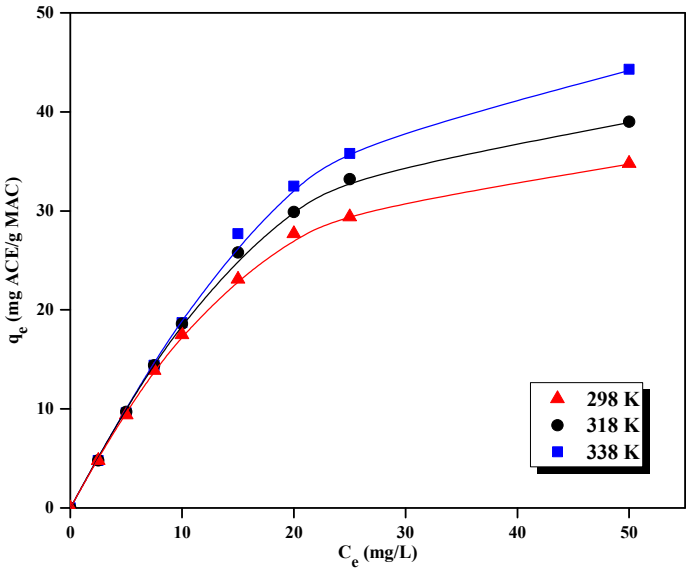

Figure 13. ACE equilibrium adsorption at different temperatures on MAC (adsorbent mass = 0.2 g·L^{-1}). Experimental points and fitting curves to the Redlich–Peterson isotherm.

Five models are used to describe the equilibrium data obtained from the adsorption isotherms of ACE on the MAC sample (Figure 13): Langmuir (Equation (7)), Freundlich (Equation (8)), Sips (Equation (9)), Redlich–Peterson (Equation (10)) and Toth (Equation (11)) [86–90].

$$q_e = \frac{q_{L.}K_{L.}C_e}{1 + K_L C_e} \quad (7)$$

$$q_e = K_F C_e^n \quad (8)$$

$$q_e = \frac{q_S (K_S C_e)^n}{1 + (K_S C_e)^n} \quad (9)$$

$$q_e = \frac{q_{RP} K_{RP} C_e}{1 + (K_{RP} C_e)^n} \quad (10)$$

$$q_e = \frac{q_T K_T C_e}{\left[1 + (K_T C_e)^n\right]^{1/n}} \quad (11)$$

where $\mathbf{q_e}$ (mg·g^{-1}) is the amount of acetaminophen adsorbed at equilibrium, $\mathbf{C_e}$ (mg·L^{-1}) is the solute concentration at equilibrium, $\mathbf{q_L}$ (mg·g^{-1}) is the Langmuir adsorption capacity, $\mathbf{K_L}$ (L·mg^{-1}) is the Langmuir constant, $\mathbf{K_F}$ (mg·g^{-1})/(L·mg^{-1})^n is the Freundlich constant, $\mathbf{n}$ (dimensionless) is the model exponent, $\mathbf{q_S}$ (mg·g^{-1}) is the Sips adsorption capacity, $\mathbf{K_S}$ (L·mg^{-1}) is the Sips constant, $\mathbf{q_{RP}}$ (mg·g^{-1}) is the Redlich–Peterson adsorption capacity, $\mathbf{K_{RP}}$ (L·mg^{-1}) is the Redlich–Peterson constant, $\mathbf{q_T}$ (mg·g^{-1}) is the Toth adsorption capacity, $\mathbf{K_T}$ (L·mg^{-1}) is the Toth constant. Tables 4 and 5 summarize the values of the two and three-parameter equilibrium models, respectively. All the models used to describe the equilibrium data fitted well with the experimental data of the adsorption isotherms (R^2 higher than 0.99) except the Freundlich model. Among them, the Redlich–Peterson model was the best one to fit the experimental data (Figure 13).

Table 4. Equilibrium model parameters of Langmuir and Freundlich for ACE adsorption on MAC.

Model	T (K)	q_L (mg·g^{-1})	K_L (L·mg^{-1})	R^2
Langmuir	298	49.0	0.056	0.9921
	318	57.0	0.050	0.9902
	338	68.9	0.040	0.9901
Model	**T (K)**	**K_F (mg·g^{-1})/(L·mg^{-1})^n**	**n**	**R^2**
Freundlich	298	3.19	0.681	0.9414
	318	3.08	0.724	0.9437
	338	2.85	0.774	0.9556

Table 5. Equilibrium model parameters of Sips, Redlich–Peterson, and Toth for ACE adsorption on MAC.

Model	T (K)	q_S (mg·g^{-1})	K_S (L·mg^{-1})	n	R^2
Sips	298	39.7	0.086	1.38	0.9991
	318	44.4	0.082	1.44	0.9992
	338	51.6	0.071	1.44	0.9987
Model	**T (K)**	**q_{RP} (mg·g^{-1})**	**K_{RP} (L·mg^{-1})**	**n**	**R^2**
Redlich–Peterson	298	64.5	0.032	1.45	0.9993
	318	75.3	0.028	1.59	0.9995
	338	87.1	0.024	1.71	0.9985
Model	**T (K)**	**q_T (mg·g^{-1})**	**K_T (L·mg^{-1})**	**n**	**R^2**
Toth	298	93.3	0.032	1.45	0.9993
	318	119.8	0.028	1.59	0.9994
	338	148.6	0.024	1.71	0.9985

To know if the adsorption process is spontaneous or not, both energy and entropy changes must be taken into account. Gibbs free energy (ΔG°, kJ·mol^{-1}), enthalpy (ΔH°, kJ·mol^{-1}), and entropy (ΔS°, J·mol^{-1}·K^{-1}) are important thermodynamic parameters whose values also explain if the adsorption process has an exothermic or endothermic nature [91]. The free energy (ΔG) of adsorption can be calculated from Equation (12):

$$\Delta G = -R \cdot T \cdot \ln K \quad (12)$$

where K was calculated from the K_{RP} values (Table 5) [92], these last obtained from the Redlich–Peterson model that gave rise to the best fitting of the experimental data [15], R is the gas constant (8.314 J·mol^{-1}·K^{-1}) and T the adsorption temperature (K). The free energy values obtained were −21.03, −22.06, and −23.00 kJ·mol^{-1} at 298, 318, and 338 K, respectively. The negative values indicate the spontaneity of the process [91]. Values of ΔG between 0 and −20 kJ·mol^{-1} suggest a physical adsorption process [92]; in this case, the ΔG values are near the minimum of this range. This result will be confirmed later by the ΔH value obtained in this work. On the other hand, enthalpy (ΔH^0) and entropy (ΔS^0) of adsorption were calculated from adsorption data at different temperatures using the van't Hoff Equation (Equation (13)) as follows:

$$\ln K = \frac{-\Delta H^0}{RT} + \frac{\Delta S^0}{R} \quad (13)$$

From the K values previously calculated and the different adsorption temperatures tested, the enthalpy and entropy of the adsorption process were calculated (Figure 14).

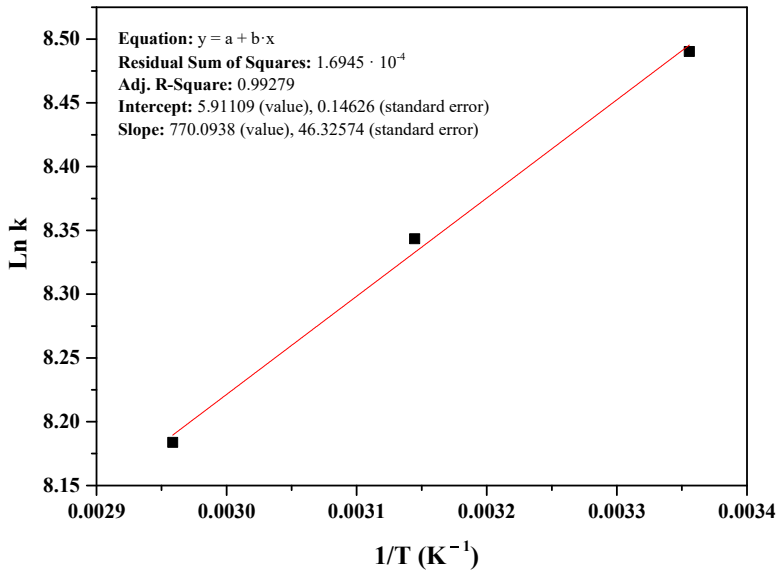

Figure 14. Van't Hoff curve for the calculation of thermodynamic parameters.

The enthalpy of adsorption is -6.4 kJ·mol^{-1}, indicating a slightly exothermic behavior. This seems to contradict the observed adsorption increase with the temperature (Figure 12), indicative of an endothermic process. This is probably due to the very small differences in the adsorption capacities at the different temperatures analyzed. Adsorption enthalpies lower than 40 kJ·mol^{-1} indicate that the process is of a physical nature and/or low-strength chemical adsorption [93]. The adsorption enthalpy value obtained in this work is similar to that reported for the ACE adsorption using activated carbons derived from Brazil nutshells ($\Delta H \approx -14$ kJ·mol^{-1}) [41]. Finally, an adsorption entropy of 49 J·mol^{-1}·K^{-1} was obtained. The positive value suggests an increase in the disorder at the solid–liquid interphase during adsorption [41,94], which could be due to the breakdown of dimers of ACE in the dissociative adsorption mechanism [95].

4. Conclusions

Homemade biochar and carbon adsorbents were synthesized from citrus waste by thermal and chemical activation with $FeCl_3$, and they were used for the removal of an emerging pollutant such as the drug acetaminophen (ACE). Among the different carbon adsorbents synthesized, the one obtained by $FeCl_3$ activation under an inert atmosphere, MAC, gave rise to the best results regarding adsorption capacity. Moreover, this material showed the added advantage of having magnetic properties that make its separation from the medium very easy. Adsorption of ACE followed the Redlich–Peterson isotherm model and Elovich model kinetics. An adsorption capacity at equilibrium at 338 K of 45 mg·g^{-1} was achieved—a similar value to other activated carbons prepared from different biomass precursors for ACE adsorption found in the literature. The free energy values obtained were in the range of -21.03 at -23.00 kJ·mol^{-1} at temperatures between 25 and 338 K, with negative values indicating the spontaneity of the process and a physical adsorption process. The calculated values of enthalpy of adsorption were -6.4 kJ·mol^{-1}, indicating a slightly exothermic behavior, while an adsorption entropy of 49 J·mol^{-1}·K^{-1} was obtained, a positive value that suggests an increase in the disorder at the solid–liquid interphase during adsorption. The fact that these carbon adsorbents come from natural waste makes this new kind of substrate more valuable, and they can be considered part of the green chemistry principles.

Author Contributions: M.G.: Conceptualization, Methodology, Validation, Investigation, Resources, Data curation, Writing (original draft, reviewing, and editing). N.A.: Conceptualization, Validation, Writing (reviewing and editing). J.B.: Conceptualization, Methodology, Software, Validation, Formal analysis, Resources, Data curation, Writing (reviewing and editing), Supervision, Project administration, Funding acquisition. C.B.: Validation, Investigation, Formal analysis, Writing (reviewing and editing), Visualization, Supervision, Project administration, Funding acquisition. C.B.M.: Conceptualization, Methodology, Software, Validation, Formal analysis, Investigation, Resources, Data curation, Writing (original draft, reviewing, and editing), Visualization, Supervision. N.M.: Conceptualization, Validation, Writing (reviewing and editing), Visualization, Supervision. All authors have read and agreed to the published version of the manuscript.

Funding: This research was funded by MCIN/AEI/10.13039/501100011033 and EU "NextGenerationEU"/PRTR through project TED 2021-129948B–I00.

Data Availability Statement: All data related to this study are available in this article or upon reasonable request.

Acknowledgments: M. Gatrouni thanks the scholarship funded by the Ministry of Higher Education and Scientific Research Carthage University to make her stay at the Universidad Autonoma of Madrid.

Conflicts of Interest: The authors declare no conflicts of interest.

References

1. Capanoglu, E.; Nemli, E.; Tomas-Barberan, F. Novel approaches in the valorization of agricultural wastes and their applications. *J. Agric. Food Chem.* **2022**, *70*, 6787–6804. [CrossRef]
2. Ahmadian, A.; Goharrizi, B.A.; Shahriari, T.; Ahmadi, S. Adsorption of chromium (VI) and Acid Orange 7 on lemon peel biochar: A response surface methodology approach. *Int. J. Environ. Sci. Technol.* **2023**, *20*, 2939–2958. [CrossRef]
3. Aljeboree, A.M.; Alshirifi, A.N.; Alkaim, A.F. Kinetics and equilibrium study for the adsorption of textile dyes on coconut shell activated carbon. *Arab. J. Chem.* **2017**, *10*, S3381–S3393. [CrossRef]
4. Balakrishna, K.; Rath, A.; Praveenkumarreddy, Y.; Guruge, K.S.; Subedi, B. A review of the occurrence of pharmaceuticals and personal care products in indian water bodies. *Ecotoxicol. Environ. Saf.* **2017**, *137*, 113–120. [CrossRef]
5. da Silva, M.D.; Schnorr, C.; Lütke, S.F.; Silva, L.F.O.; Manera, C.; Perondi, D.; Godinho, M.; Collazzo, G.C.; Dotto, G.L. Citrus fruit residues as alternative precursors to developing H_2O and CO_2 activated carbons and its application for Cu(II) adsorption. *Environ. Sci. Pollut. Res.* **2023**, *30*, 63661–63677. [CrossRef]
6. Kumar, L.; Yadav, V.; Yadav, M.; Saini, N.; Jagannathan, K.; Murugesan, V.; Ezhilsevi, V. Systematic studies on the effect of structural modification of orange peel for remediation of phenol contaminated water. *Water Environ. Res.* **2023**, *95*, e10872. [CrossRef]
7. Awogbemi, O.; Kallon, D.V.V. Pretreatment techniques for agricultural waste. *Case Stud. Chem. Environ. Eng.* **2022**, *6*, 100229. [CrossRef]
8. Tran, H.N.; Tomul, F.; Ha, N.T.H.; Nguyen, D.T.; Lima, E.C.; Le, G.T.; Chang, C.T.; Masindi, V.; Woo, S.H. Innovative spherical biochar for pharmaceutical removal from water: Insight into adsorption mechanism. *J. Hazard. Mater.* **2020**, *394*, 122255. [CrossRef]
9. Chakraborty, R.; Pradhan, M.; Nayak, A.K.; Nayak, A.K. Recent advancement of biomass-derived porous carbon based materials for energy and environmental remediation applications. *J. Mater. Chem.* **2022**, *10*, 6965–7005.
10. Patel, M.; Kumar, R.; Pittman, C.U., Jr.; Mohan, D. Ciprofloxacin and acetaminophen sorption onto banana peel biochars: Environmental and process parameter influences. *Environ. Res.* **2021**, *201*, 111218. [CrossRef]
11. Verma, L.; Siddiquea, M.A.; Singh, J.; Bharagava, R.N. As(III) and As(V) removal by using iron impregnated biosorbents derived from waste biomass of Citrus limmeta (peel and pulp) from the aqueous solution and ground water. *J. Environ. Manag.* **2019**, *250*, 109452. [CrossRef]
12. Babu, S.; Rathore, S.S.; Singh, R.; Kumar, S.; Singh, V.K.; Yadav, S.K.; Yadav, V.; Raj, R.; Yadav, D.; Shekhawat, K.; et al. Exploring agricultural waste biomass for energy, food and feed production and pollution mitigation: A review. *Bioresour. Technol.* **2022**, *360*, 127566. [CrossRef]
13. Marsh, H.; Rodríguez-Reinoso, F. *Activated Carbon*; Elsevier Ltd.: Amsterdam, The Netherlands, 2006; ISBN 9780080444635.
14. Bedia, J.; Peñas-Garzón, M.; Gómez-Avilés, A.; Rodriguez, J.J.; Belver, C. Review on Activated Carbons by Chemical Activation with $FeCl_3$. *J. Carbon Res.* **2020**, *6*, 21. [CrossRef]
15. Gomez-Aviles, A.; Penas-Garzon, M.; Belver, C.; Rodriguez, J.J.; Bedia, J. Equilibrium, kinetics and breakthrough curves of acetaminophen adsorption onto activated carbons from microwave-assisted $FeCl_3$-activation of lignin. *Sep. Purif. Technol.* **2022**, *278*, 119654. [CrossRef]

16. Cesano, F.; Cravanzola, S.; Brunella, V.; Damin, A.; Scarano, D. From Polymer to Magnetic Porous Carbon Spheres: Combined Microscopy, Spectroscopy, and Porosity Studies. *Front. Mater.* **2019**, *6*, 84. [CrossRef]
17. Demarchi, C.A.; Michel, B.S.; Nedelko, N.; S'lawska-Waniewska, A.; Dłuzewski, P.; Kaleta, A.; Minikayev, R.; Strachowski, T.; Lipinska, L.; Dal Magro, J.; et al. Preparation, characterization, and application of magnetic activated carbon from termite feces for the adsorption of Cr(VI) from aqueous solutions. *Powder Technol.* **2019**, *354*, 432–441. [CrossRef]
18. Holmes, A.M.; Mackenzie, L.; Roberts, M.S. Disposition and measured toxicity of zinc oxide nanoparticles and zinc ions against keratinocytes in cell culture and viable human epidermis. *Nanotoxicology* **2020**, *14*, 263–274. [CrossRef]
19. Ye, N.; Wang, Z.; Wang, S.; Peijnenburg, W.J.G.M. Toxicity of mixtures of zinc oxide and graphene oxide nanoparticles to aquatic organisms of different trophic level: Particles outperform dissolved ions. *Nanotoxicology* **2018**, *12*, 423–438. [CrossRef]
20. Xu, Z.; Sun, Z.; Zhou, Y.; Chen, W.; Zhang, T.; Huang, Y.; Zhang, D. Insights into the pyrolysis behavior and adsorption properties of activated carbon from waste cotton textiles by $FeCl_3$-activation. *Colloids Surf. A Physicochem. Eng. Asp.* **2019**, *582*, 123934. [CrossRef]
21. Xu, Z.; Zhou, Y.; Sun, Z.; Zhang, D.; Huang, Y.; Gu, S.; Chen, W. Understanding reactions and pore-forming mechanisms between waste cotton woven and $FeCl_3$ during the synthesis of magnetic activated carbon. *Chemosphere* **2020**, *241*, 125120. [CrossRef]
22. Bansal, R.C.; Goyal, M. *Activated Carbon Adsorption*; CRC Press: Boca Raton, FL, USA, 2005; ISBN 9781420028812.
23. Palomo, J.; Rodríguez-Cano, M.A.; Rodríguez-Mirasol, J.; Cordero, T. On the kinetics of methanol dehydration to dimethyl ether on Zr-loaded P-containing mesoporous activated carbon catalyst. *Chem. Eng. J.* **2019**, *378*, 122198. [CrossRef]
24. Fang, R.; Huang, H.; Ji, J.; He, M.; Feng, Q.; Zhan, Y.; Leung, D.Y.C. Effcient MnOx supported on coconut shell activated carbon for catalytic oxidation of indoor formaldehyde at room temperature. *Chem. Eng. J.* **2018**, *334*, 2050–2057. [CrossRef]
25. Bedia, J.; Ruiz-Rosas, R.; Rodríguez-Mirasol, J.; Cordero, T. Kinetic study of the decomposition of 2-butanol on carbon-based acid catalyst. *AIChE J.* **2010**, *56*, 1557–1568. [CrossRef]
26. Valero-Romero, M.J.; Calvo-Muñoz, E.M.; Ruiz-Rosas, R.; Rodríguez-Mirasol, J.; Cordero, T. Phosphorus-Containing Mesoporous Carbon Acid Catalyst for Methanol Dehydration to Dimethyl Ether. *Ind. Eng. Chem. Res.* **2019**, *58*, 4042–4053. [CrossRef]
27. Chen, C.; Mi, S.; Lao, D.; Shi, P.; Tong, Z.; Li, Z.; Hu, H. Single-step synthesis of eucalyptus sawdust magnetic activated carbon and its adsorption behavior for methylene blue. *RSC Adv.* **2019**, *9*, 22248–22262. [CrossRef]
28. Tian, D.; Xu, Z.; Zhang, D.; Chen, W.; Cai, J.; Deng, H.; Sun, Z.; Zhou, Y. Micro–mesoporous carbon from cotton waste activated by $FeCl_3/ZnCl_2$: Preparation, optimization, characterization and adsorption of methylene blue and eriochrome black T. *J. Solid State Chem.* **2019**, *269*, 580–587. [CrossRef]
29. Cazetta, A.L.; Pezoti, O.; Bedin, K.C.; Silva, T.L.; Paesano Junior, A.; Asefa, T.; Almeida, V.C. Magnetic Activated Carbon Derived from Biomass Waste by Concurrent Synthesis: Efficient Adsorbent for Toxic Dyes. *ACS Sustain. Chem. Eng.* **2016**, *4*, 1058–1068. [CrossRef]
30. Ahmed, M.J.; Theydan, S.K. Adsorptive removal of p-nitrophenol on microporous activated carbon by $FeCl_3$ activation: Equilibrium and kinetics studies. *Desalin. Water Treat.* **2015**, *55*, 522–531. [CrossRef]
31. Mojoudi, N.; Soleimani, M.; Mirghaffari, N.; Belver, C.; Bedia, J. Removal of phenol and phosphate from aqueous solutions using activated carbons prepared from oily sludge through physical and chemical activation. *Water Sci. Technol.* **2019**, *80*, 575–586. [CrossRef]
32. Qiu, L.; Suo, C.; Zhang, N.; Yuan, R.; Chen, H.; Zhou, B. Adsorption of heavy metals by activated carbon: Effect of natural organic matter and regeneration methods of the adsorbent. *Desal. Water Treat.* **2022**, *252*, 148–166. [CrossRef]
33. Sultana, M.; Rownok, M.H.; Sabrin, M.; Rahaman, M.H.; Nur Alam, S.M. A review on experimental chemically modified activated carbon to enhance dye and heavy metals adsorption. *Clean. Eng. Technol.* **2022**, *6*, 100382. [CrossRef]
34. Kumar, A.; Patra, C.; Kumar Rajendran, H.; Narayanasamy, S. Activated carbon-chitosan based adsorbent for the efficient removal of the emerging contaminant diclofenac: Synthesis, characterization and phytotoxicity studies. *Chemosphere* **2022**, *307*, 135806. [CrossRef]
35. Sellaoui, L.; Gomez-Aviles, A.; Dhaouadi, F.; Bedia, J.; Bonilla-Petriciolet, A.; Rtimi, S.; Belver, C. Adsorption of emerging pollutants on lignin-based activated carbon: Analysis of adsorption mechanism via characterization, kinetics and equilibrium studies. *Chem. Eng. J.* **2023**, *452*, 139399. [CrossRef]
36. Peña-Guzman, C.; Ulloa-Sanchez, S.; Mora, K.; Helena-Bustos, R.; Lopez-Barrera, E.; Alvarez, J.; Rodriguez-Pinzon, M. Emerging pollutants in the urban water cycle in Latin America: A review of the current literature. *J. Environ. Manag.* **2019**, *237*, 408–423. [CrossRef]
37. Farre, M.; Perez, S.; Kantiani, L.; Barcelo, D. Fate and toxicity of emerging pollutants, their metabolites and transformation products in the aquatic environment. *TrAC Trends Anal. Chem.* **2008**, *27*, 991–1007. [CrossRef]
38. Fu, K.; Yue, Q.; Gao, B.; Sun, Y.; Wang, Y.; Li, Q.; Zhao, P.; Chen, S. Physicochemical and adsorptive properties of activated carbons from Arundo donax Linn utilizing different iron salts as activating agents. *J. Taiwan Inst. Chem. Eng.* **2014**, *45*, 3007–3015. [CrossRef]
39. Bedia, J.; Belver, C.; Ponce, S.; Rodriguez, J.; Rodriguez, J.J. Adsorption of antipyrine by activated carbons from $FeCl_3$-activation of Tara gum. *Chem. Eng. J.* **2018**, *333*, 58–65. [CrossRef]
40. Diaz, E.; Manzano, F.J.; Villamil, J.; Rodriguez, J.J.; Mohedano, A.F. Low-Cost Activated Grape Seed-Derived Hydrochar through Hydrothermal Carbonization and Chemical Activation for Sulfamethoxazole Adsorption. *Appl. Sci.* **2019**, *9*, 5127. [CrossRef]

41. Lima, D.R.; Hosseini-Bandegharaei, A.; Thue, P.S.; Lima, E.C.; de Albuquerque, Y.R.T.; dos Reis, G.S.; Umpierres, C.S.; Dias, S.L.P.; Tran, H.N. Efficient acetaminophen removal from water and hospital effluents treatment by activated carbons derived from Brazil nutshells. *Colloids Surf. A* **2019**, *583*, 123966. [CrossRef]
42. Murray, K.E.; Thomas, S.M.; Boduor, A.A. Prioritizing research for trace pollutants and emerging contaminants in the freshwater environment. *Environ. Pollut.* **2010**, *158*, 3462–3471. [CrossRef]
43. Islam, M.A.; Nazal, M.K.; Sajidm, M.; Suliman, M.A. Adsorptive removal of paracetamol from aqueous media: A review of adsorbent materials, adsorption mechanisms, advancements, and future perspectives. *J. Mol. Liq.* **2024**, *396*, 123976. [CrossRef]
44. Aus der Beek, T.; Weber, F.A.; Bergmann, A.; Hickmann, S.; Ebert, I.; Hein, A.; Küster, A. Pharmaceuticals in the environment—Global occurrences and perspectives. *Environ. Toxicol. Chem.* **2016**, *35*, 823–835. [CrossRef]
45. Barasarathi, J.; Abdullah, P.S.; Uche, E.C. Application of magnetic carbon nanocomposite from agro-waste for the removal of pollutants from water and wastewater. *Chemosphere* **2022**, *305*, 135384. [CrossRef]
46. Kleywegt, S.; Payne, M.; Ng, F.; Fletcher, T. Environmental loadings of active pharmaceutical ingredients from manufacturing facilities in Canada. *Sci. Total Environ.* **2019**, *646*, 257–264. [CrossRef]
47. Nguyen, D.V.; Nguyen, H.M.; Bui, Q.L.N.; Do, T.V.T.; Lam, H.H.; Tran-Thuy, T.-M.; Nguyen, L.Q. Magnetic Activated Carbon from $ZnCl_2$ and $FeCl_3$ Coactivation of Lotus Seedpod: One-Pot Preparation, Characterization, and Catalytic Activity towards Robust Degradation of Acid Orange 10. *Bioinorg. Chem. Appl.* **2023**, *2023*, 3848456. [CrossRef]
48. Jagiello, J.; Ania, C.; Parra, J.B.; Cook, C. Dual gas analysis of microporous carbons using 2D-NLDFT heterogeneous surface model and combined adsorption data of N_2 and CO_2. *Carbon* **2015**, *91*, 330–337. [CrossRef]
49. Issa, A.A.; Al-Degs, Y.S.; Al-Ghouti, M.A.; Olimat, A.A.M. Studying competitive sorption behavior of methylene blue and malachite green using multivariate calibration. *Chem. Eng. J.* **2014**, *240*, 554–564. [CrossRef]
50. Aboli, E.; Jafari, D.; Esmaeili, H. Heavy metal ions (lead, cobalt, and nickel) biosorption from aqueous solution onto activated carbon prepared from Citrus limetta leaves. *Carbon Lett.* **2020**, *30*, 683–698. [CrossRef]
51. Chaudhary, H.; Dinakaran, J.; Notup, T.; Vikram, K.; Rao, K.S. Comparison of Adsorption Performance of Biochar Derived from Urban Biowaste Materials for Removal of Heavy Metals. *Environ. Manag.* **2024**, *73*, 408–424. [CrossRef]
52. Lee, S.-M.; Lee, S.-H.; Roh, J.-S. Analysis of Activation Process of Carbon Black Based on Structural Parameters Obtained by XRD Analysis. *Crystals* **2021**, *11*, 153. [CrossRef]
53. Depci, T. Comparison of activated carbon and iron impregnated activated carbon derived from Golbasi lignite to remove cyanide from water. *Chem. Eng. J.* **2012**, *181*, 467–478. [CrossRef]
54. Anyika, C.; Asri, N.A.M.; Majid, Z.A.; Yahya, A.; Jaafar, J. Synthesis and characterization of magnetic activated carbon developed from palm kernel shells. *Nanotechnol. Environ. Eng.* **2017**, *2*, 16. [CrossRef]
55. Ibrahim, M.; Siddiqe, A.; Verma, L.; Singh, J.; Koduru, J.R. Adsorptive removal of fluoride from aqueous solution by biogenic iron permeated activated carbon derived from sweet lime waste. *Acta Chim. Slov.* **2019**, *66*, 123–135. [CrossRef]
56. Lunge, S.; Singh, S.; Sinha, A. Magnetic iron oxide (Fe_3O_4) nano-particles from tea waste for arsenic removal. *J. Magn. Magn. Mater.* **2014**, *356*, 21–31. [CrossRef]
57. Hosakun, Y.; Halász, K.; Horváth, M.; Csóka, L.; Djokovic, V. ATR-FTIR study of the interaction of CO_2 with bacterial cellulose-based membranes. *Chem. Eng. J.* **2017**, *324*, 83–92. [CrossRef]
58. Mastalerz, M.; Goodman, A.; Chirdon, D. Coal Lithotypes before, during, and after Exposure to CO2: Insights from Direct Fourier Transform Infrared Investigation. *Energy Fuels* **2012**, *26*, 3586–3591. [CrossRef]
59. Thines, K.R.; Abdullah, E.C.; Mubarak, N.M.; Ruthiraan, M. In-situ polymerization of magnetic-biochar-polypyrrole composite: A novel application in supercapacitor. *Biomass Bioenergy* **2017**, *98*, 95–111. [CrossRef]
60. Mohan, D.; Sarswat, A.; Singh, V.K.; Alexandre-Franco, M.; Pittman, C. Development of magnetic activated carbon from almond shells for trinitrophenol removal from water. *Chem. Eng. J.* **2011**, *172*, 1111–1125. [CrossRef]
61. Lawal, I.A.; Klink, M.; Ndungu, P. Deep eutectic solvent as an efficient modifier of low-cost adsorbent for the removal of pharmaceuticals and dye. *Environ. Res.* **2019**, *179*, 108837. [CrossRef]
62. Menendez, J.A.; Illan-Gomez, M.J.; Leon, C.A.L.; Radovic, L.R. On the difference between the isoelectric point and the point of zero charge of carbons. *Carbon* **1995**, *33*, 1655–1657. [CrossRef]
63. Nguyen, D.T.; Tran, H.N.; Juang, R.S.; Dat, N.D.; Tomul, F.; Ivanets, A.; Woo, S.H.; Hosseini-Bandegharaei, A.; Nguyen, V.P.; Chao, H.P. Adsorption process and mechanism of acetaminophen onto commercial activated carbon. *J. Environ. Chem. Eng.* **2020**, *8*, 104408. [CrossRef]
64. Cui, H.-J.; Cai, J.-K.; Zhao, H.; Yuan, B.; Ai, C.; Fu, M.-L. One step solvothermal synthesis of functional hybrid γ-Fe_2O_3/carbon hollow spheres with superior capacities for heavy metal removal. *J. Colloid Interface Sci.* **2014**, *425*, 131–135. [CrossRef]
65. Ramya, V.; Murugan, D.; Lajapathirai, C.; Meenatchisundaram, S. A composite adsorbent of superparamagnetic nanoparticles with sludge biomass derived activated carbon for the removal of chromium (VI). *J. Cleaner Prod.* **2022**, *366*, 132853. [CrossRef]
66. Zhu, Y.; Wang, Y.; Wang, T.; Liu, H.; Liu, H.; Zang, M. One-step preparation of coal-based magnetic activated carbon with hierarchically porous structure and easy magnetic separation capability for adsorption applications. *J. Magn. Magn. Mater.* **2023**, *569*, 170480. [CrossRef]
67. Ranjithkumar, V.; Sangeetha, S.; Vairam, S. Synthesis of magnetic activated carbon/α-Fe_2O_3 nanocomposite and its application in the removal of acid yellow 17 dye from water. *J. Hazard. Mater.* **2014**, *273*, 127–135. [CrossRef]

68. Zhang, S.W.; Zeng, M.Y.; Li, J.X.; Li, J.; Xu, J.Z.; Wang, X.K. Porous magnetic carbon sheets from biomass as an adsorbent for the fast removal of organic pollutants from aqueous solution. *J. Mater. Chem. A* **2014**, *2*, 4391–4397. [CrossRef]
69. Wamba, A.G.N.; Lima, E.C.; Ndi, S.K.; Thue, P.S.; Kayem, J.G.; Rodembusch, F.S.; dos Reis, G.S.; de Alencar, W.S. Synthesis of grafted natural pozzolan with 3-aminopropyltriethoxysilane: Preparation, characterization, and application for removal of Brilliant Green 1 and Reactive Black 5 from aqueous solutions. *Environ. Sci. Pollut. Res.* **2017**, *24*, 21807–21820. [CrossRef]
70. Spessato, L.; Bedin, K.C.; Cazetta, A.L.; Souza, I.P.; Duarte, V.A.; Crespo, L.H.; Silva, M.C.; Pontes RMAlmeida, V.C. KOH-super activated carbon from biomass waste: Insights into the paracetamol adsorption mechanism and thermal regeneration cycles. *J. Hazard. Mater.* **2019**, *371*, 499–505. [CrossRef]
71. Tran, H.N.; You, S.-J.; Chao, H.-P. Fast and efficient adsorption of methylene green 5 on activated carbon prepared from new chemical activation method. *J. Environ. Manag.* **2017**, *188*, 322–336. [CrossRef]
72. Boakye, P.; Tran, H.N.; Lee, D.S.; Woo, S.H. Effect of water washing pretreatment on property and adsorption capacity of macroalgae-derived biochar. *J. Environ. Manag.* **2019**, *233*, 165–174. [CrossRef]
73. Ninh, P.T.T.; Ngoc Tuyen, L.T.; Dat, N.D.; Nguyen, M.L.; Dong, N.T.; Chao, H.-P.; Tran, H.N. Two-stage preparation of highly mesoporous carbon for super-adsorption of paracetamol and tetracycline in water: Important contribution of pore filling and π-π interaction. *Environ. Res.* **2023**, *218*, 114927. [CrossRef]
74. Wang, J.; Guo, X. Adsorption kinetic models: Physical meanings, applications, and solving methods. *J. Hazard. Mater.* **2020**, *390*, 122156. [CrossRef]
75. Mohammadi, S.Z.; Darijani, Z.; Karimi, M.A. Fast and efficient removal of phenol by magnetic activated carbon-cobalt nanoparticles. *J. Alloys Compd.* **2020**, *832*, 154942. [CrossRef]
76. da Silva, M.C.F.; Lütke, S.F.; Nascimento, V.X.; Lima, E.C.; Silva, L.F.O.; Oliveira, M.L.S.; Dotto, G.L. Activated carbon prepared from Brazil nut shells towards phenol removal from aqueous solutions. *Environ. Sci. Pollut. Res.* **2023**, *30*, 82795–82806. [CrossRef]
77. Giles, C.H.; Smith, D.; Huitson, A. A general treatment and classification of the solute adsorption isotherm. I. Theoretical. *J. Colloid Interface Sci.* **1974**, *47*, 755–765. [CrossRef]
78. Galhetas, M.; Mestre, A.S.; Pinto, M.L.; Gulyurtlu, I.; Lopes, H.; Carvalho, A.P. Carbon-based materials prepared from pine gasification residues for acetaminophen adsorption. *Chem. Eng. J.* **2014**, *240*, 344–351. [CrossRef]
79. Garcia-Mateos, F.J.; Ruiz-Rosas, R.; Marques, M.D.; Cotoruelo, L.M.; Rodriguez- Mirasol, J.; Cordero, T. Removal of paracetamol on biomass-derived activated carbon: Modeling the fixed bed breakthrough curves using batch adsorption experiments. *Chem. Eng. J.* **2015**, *279*, 18–30. [CrossRef]
80. Moussavi, G.; Hossaini, Z.; Pourakbar, M. High-rate adsorption of acetaminophen from the contaminated water onto double-oxidized graphene oxide. *Chem. Eng. J.* **2016**, *287*, 665–673. [CrossRef]
81. Coimbra, R.N.; Calisto, V.; Ferreira, C.I.A.; Esteves, V.I.; Otero, M. Removal of pharmaceuticals from municipal wastewater by adsorption onto pyrolyzed pulp mill sludge. *Arab. J. Chem.* **2015**, *12*, 3611–3620. [CrossRef]
82. Nche, N.A.G.; Bopda, A.; Tchuifon, D.R.T.; Ngakou, C.S.; Kuete, I.-H.T.; Gabche, A.S. Removal of paracetamol from aqueous solution by adsorption onto activated carbon prepared from rice husk. *J. Chem. Pharm. Res.* **2017**, *9*, 56–68.
83. Nourmoradi, H.; Moghadam, K.F.; Jafari, A.; Kamarehie, B. Removal of acetaminophen and ibuprofen from aqueous solutions by activated carbon derived from Quercus brantii (Oak) acorn as a low-cost biosorbent. *J. Environ. Chem. Eng.* **2018**, *6*, 6807–6815. [CrossRef]
84. Mestre, A.S.; Pires, R.A.; Aroso, I.; Fernandes, E.M.; Pinto, M.L.; Reis, R.L.; Andrade, M.A.; Pires, J.; Silva, S.P.; Carvalho, A.P. Activated carbons prepared from industrial pre-treated cork: Sustainable adsorbents for pharmaceutical compounds removal. *Chem. Eng. J.* **2014**, *253*, 408–417. [CrossRef]
85. Mestre, A.S.; Bexiga, A.S.; Proença, M.; Andrade, M.; Pinto, M.L.; Matos, I.; Fonseca, I.M.; Carvalho, A.P. Activated carbons from sisal waste by chemical activation with K_2CO_3: Kinetics of paracetamol and ibuprofen removal from aqueous solution. *Bioresour. Technol.* **2011**, *102*, 8253–8260. [CrossRef]
86. Langmuir, I. The adsorption of gases on plane surfaces of glass, mica and platinum. *J. Am. Chem. Soc.* **1918**, *40*, 1361–1403. [CrossRef]
87. Freundlich, H. Über die Adsorption in Lösungen. *Zeitschrift Für Phys. Chemie* **1906**, *57*, 385–471. [CrossRef]
88. Sips, R. On the structure of a catalyst surface. *J. Chem. Phys.* **1948**, *16*, 490–495. [CrossRef]
89. Redlich, O.; Peterson, D.L. A useful adsorption isotherm. *J. Phys. Chem.* **1959**, *63*, 1024. [CrossRef]
90. Toth, J. State Equation of the Solid-Gas Interface Layers. *Acta Chim. Hung.* **1971**, *69*, 311–328.
91. Lima, E.C.; Hosseini-Bandegharaei, A.; Moreno-Pirajan, J.C.; Anastopoulos, I. A critical review of the estimation of the thermodynamic parameters on adsorption equilibria. Wrong use of equilibrium constant in the Van't Hoof equation for calculation of thermodynamic parameters of adsorption. *J. Mol. Liq.* **2019**, *273*, 425–434. [CrossRef]
92. Almeida, C.A.P.; Debacher, N.A.; Downs, A.J.; Cottet, L.; Mello, C.A.D. Removal of methylene blue from colored effluents by adsorption on montmorillonite clay. *J. Colloid Interface Sci.* **2009**, *332*, 46–53. [CrossRef]
93. Chang, R.; Thoman, J.W., Jr. *Intermolecular Forces. Chapter 17. Physical Chemistry for Chemical Sciences*; University Science Books: Sausalito, CA, USA, 2014; pp. 779–808.

94. Wang, R.Z.; Huang, D.L.; Liu, Y.G.; Zhang, C.; Lai, C.; Wang, X.; Zeng, G.M.; Zhang, Q.; Gong, X.M.; Xu, P. Synergistic removal of copper and tetracycline from aqueous solution by steam-activated bamboo-derived biochar. *J. Hazard. Mater.* **2020**, *384*, 121470. [CrossRef]
95. Saha, P.; Chowdhury, S. Insight Into Adsorption Thermodynamics. In *Thermodynamics*; InTech: Vienna, Austria, 2011; pp. 349–364. [CrossRef]